Nuclear Instruments and Methods in Physics Research A 622 (2010) 261–269

Contents lists available at ScienceDirect

Nuclear Instruments and Methods in Physics Research A

journal homepage: www.elsevier.com/locate/nima

Development of a compact and high spatial resolution gamma camera system using $LaBr_3$(Ce)

Seiichi Yamamoto [a,*], Masao Imaizumi [b], Eku Shimosegawa [b], Jun Hatazawa [b]

[a] Kobe City College of Technology, 8-3 Gakuen-Higashi-machi, Nishi-ku, Kobe 651-2194, Japan
[b] Department of Nuclear Medicine and Tracer Kinetics, Osaka University Graduate School of Medicine, Japan

ARTICLE INFO

Article history:
Received 2 May 2010
Received in revised form
3 July 2010
Accepted 6 July 2010
Available online 14 July 2010

Keywords:
Gamma camera
$LaBr_3$(Ce)
High resolution

ABSTRACT

In small animal imaging using a single photon emitting radionuclide, a high spatial resolution gamma camera is required. However, its spatial resolution is limited by the light output of conventional scintillators such as NaI(Tl). We developed and tested a small field-of-view (FOV) gamma camera using a new scintillator, $LaBr_3$(Ce). The $LaBr_3$(Ce) gamma camera consists of a 2 mm thick $LaBr_3$(Ce) scintillator, a 2 in. 8×8 multi-anode position sensitive photomultiplier tube (Hamamatsu H8500), and a personal computer-based data acquisition system. The $LaBr_3$(Ce) scintillator was directly coupled to the PSPMT and was contained in a hermetically shielded and light tight aluminum case. The signals from the PSPMT were gain corrected, weighted summed, and digitized by 100 MHz free running A-D converters in the data acquisition system. The detector part of the gamma camera was encased in a tungsten gamma shield, and a tungsten pinhole collimator was mounted in front of the detector surface. The intrinsic spatial resolution that was measured using a tungsten slit mask was 0.75 mm FWHM, and the energy resolution was 8.9% FWHM for 122 keV gamma photons. We obtained transmission and emission images that demonstrated the high spatial resolution of the gamma camera system. Approximately two years after the fabrication of the detector, the flood image showed significant distortion due to the change in $LaBr_3$(Ce) of its hygroscopic characteristic. These results confirm that the developed $LaBr_3$(Ce) gamma camera is promising for small animal imaging using a low energy single photon emitting radionuclide if the hygroscopic problem of $LaBr_3$(Ce) will be solved.

1. Introduction

In small animal imaging using a single photon emitting radionuclide, a high spatial resolution gamma camera is required [1,2]. To obtain high spatial resolution in small animal imaging, pinhole collimators are combined with large field-of-view (FOV) NaI(Tl) gamma cameras, and a magnification technique is usually used [3]. Although these gamma camera systems showed excellent small animal images, the size of the camera system is huge because they employed gamma cameras for human imaging. To reduce the size of gamma camera systems while maintaining the system spatial resolution, the intrinsic spatial resolution of the camera must be improved.

One of the major factors for limiting the intrinsic spatial resolution of gamma cameras is the light output of the scintillator used for the system [4]. Most gamma cameras employed a NaI(Tl) scintillator for the relatively large light output. The intrinsic resolution of NaI(Tl) gamma cameras combined with 2 in. round photomultiplier tubes is limited to be approximately 3 mm FWHM and that of the small FOV NaI(Tl) gamma cameras combined with a position sensitive photomultiplier tube (PSPMT) is limited to approximately 1.5 mm [5]. For improving the spatial resolution of small FOV gamma cameras, using an optical fiber plate, is one solution [5]. This gamma camera using an optical fiber plate consisted of an NaI(Tl) scintillator optically coupled to a PSPMT. The small FOV gamma camera used an optical fiber plate to reduce the scintillation light spread of NaI(Tl). Thus reducing the scintillation light spread improves the spatial resolution of PSPMT-based gamma cameras. However, spatial resolution was limited to 1 mm FWHM even with an optical fiber plate and 2 mm thick NaI(Tl) scintillator [5]. If we could use scintillator with high light output, we may be able to improve the spatial resolution of the PSPMT-based gamma camera.

$LaBr_3$(Ce) is a new scintillator with approximately 1.7 times larger light output than NaI(Tl), short decay time of 16 ns, and relatively high density of 5.1 [6,7]. Kurn et al. [8] used $LaBr_3$(Ce) for a time-of-flight (TOF) PET system using the property of short decay time. However, the properties of $LaBr_3$(Ce) are also suitable for low energy single photon emitting radionuclide such as Tc-99 m (140 keV), I-123 (159 keV), or Tl-201 (70 keV) imaging

* Corresponding author.
E-mail address: s-yama@kobe-kosen.ac.jp (S. Yamamoto).

0168-9002/$ - see front matter © 2010 Elsevier B.V. All rights reserved.
doi:10.1016/j.nima.2010.07.038

systems where high spatial resolution and energy resolution are required. The high light output will improve the spatial resolution and energy resolution of the gamma camera. The relatively high density of $LaBr_3$(Ce) can reduce the thickness of the scintillator that also improves the spatial resolution. $LaBr_3$(Ce) was also used for a scinti-mammography application [9,10]. A relatively large sized pixilated $LaBr_3$(Ce) based gamma camera has also been reported [11]. However, some of these researches did not use the potential of $LaBr_3$(Ce) to improve the spatial resolution.

Other approaches for high spatial resolution imaging of single photon emitting radionuclide are the use of semiconductor detectors [12,13]. These semiconductor detectors directly convert the gamma photons to electrons. However, the spatial resolution is determined by the pixel sizes of these semiconductor detectors and the application specific integrated circuit (ASIC), which is usually high cost for the development, is needed for the front end electronics.

In this paper, we report a small FOV $LaBr_3$(Ce) gamma camera that directly couples $LaBr_3$(Ce) to PSPMT to improve the spatial resolution. We show its design, performance, and images for molecular imaging researches. We also show long term stability of the developed $LaBr_3$(Ce) gamma camera.

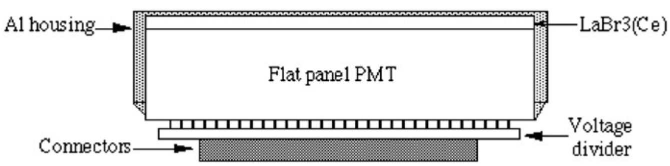

Fig. 1. Cross-sectional view of detector part of $LaBr_3$(Ce) gamma camera.

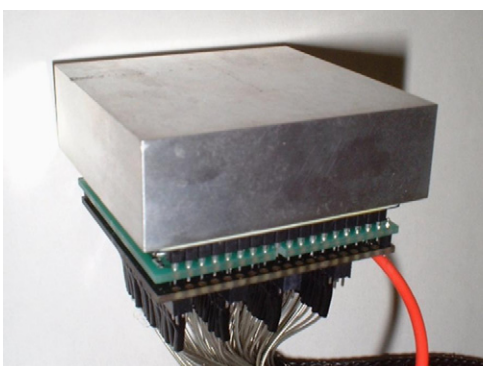

Fig. 2. Photograph of detector part of LaBr3(Ce) gamma camera.

2. Materials and methods

2.1. System description

Fig. 1 shows a cross-sectional view of the detector part of our developed $LaBr_3$(Ce) gamma camera that consists of a 2 mm thick $LaBr_3$(Ce) scintillator (Saint Gobain, BrilLanCe 380, USA) and a 25.4 mm (2 in.) square multi-anode PSPMT (Hamamatsu H8500: Hamamatsu Photonix, Hamamatsu, Japan). The $LaBr_3$(Ce) scintillator, which was directly coupled to the PSPMT by its manufacturer (Saint Gobain), was contained in a hermetically and light sealed aluminum case. The detection efficiency of 2 mm thick $LaBr_3$(Ce) scintillator for Tc-99 m gamma photons (141 keV) was around 40% [7].

The size of $LaBr_3$(Ce) is 50.8 mm $\times$ 50.8 mm $\times$ 2 mm and the front surface (upper side of Fig. 1) was covered by a white reflector, and the sides were painted black to reduce the stray light in the scintillator. The thickness of the front aluminum case was 0.5 mm.

A photograph of the detector part of the $LaBr_3$(Ce) gamma camera is shown in Fig. 2. The size of the detector is 58 mm $\times$ 58 mm $\times$ 32.5 mm. Signals from the anodes of the PSPMT are read out by 64 coaxial cables and fed to the gain control amplifiers.

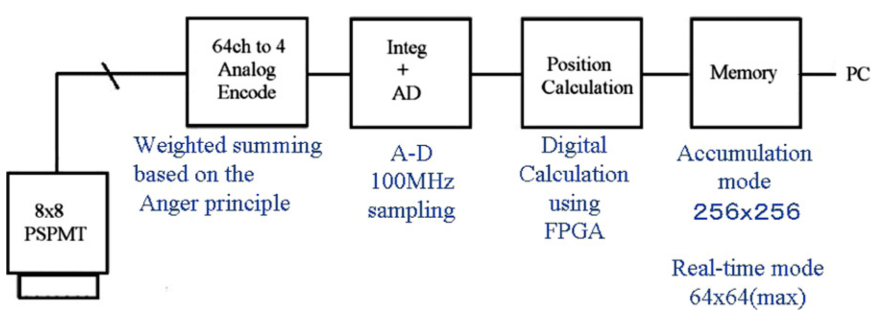

Fig. 3. Electronics and data acquisition system of developed $LaBr_3$(Ce) gamma camera.

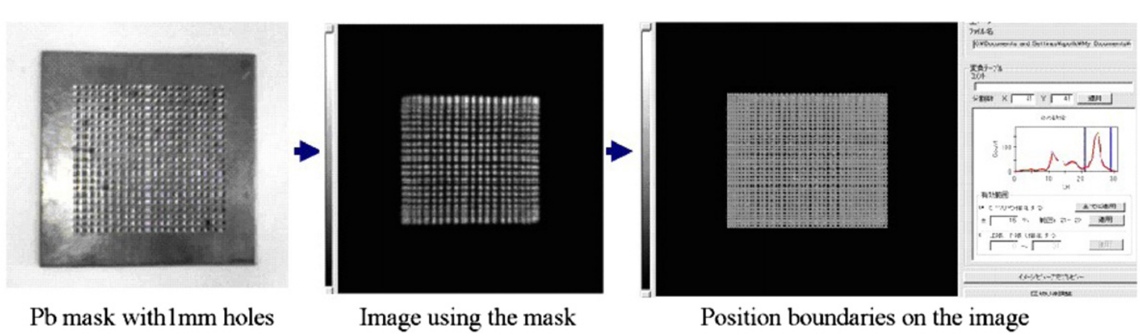

Fig. 4. Schematic diagram of position boundary setting of developed $LaBr_3$(Ce) gamma camera.

A block diagram of the electronics circuit and the data acquisition system is shown in Fig. 3. The gain control amplifiers were used to tune the gain variations of the PSPMT anodes to be approximately within 20%. The outputs of the gain controlled amplifiers are fed to weighted summing amplifiers and digitized by 100 MHz free running A-D converters. Digitally calculated position and energy are accumulated in the memory and transferred to a personal computer. The data acquisition system resembles the previously reported PET/SPECT imaging system [14].

The acquisition system has two modes: one is a high spatial resolution accumulation mode with a 256×256 matrix without flood and linearity correction with the pixel size of 0.3 mm. The other is a corrected mode with a 41×41 matrix with energy, linearity, and flood corrections were made with the pixel size of 1 mm.

In Fig. 4, a schematic diagram of the position boundary and energy window settings for the corrected mode of the developed $LaBr_3$(Ce) gamma camera is shown. A 2 mm thick lead mask with 21×21, 1 mm holes, 1 mm walls (Fig. 4-left) was used to acquire the data for the position boundary and energy window settings. The mask was positioned on the gamma camera, 122 keV gamma photons from Co-57 were uniformly irradiated, and images of the holes were accumulated (Fig. 4-center). We set 41×41 position boundaries on the image from the peaks and valleys of the holes of the image (Fig. 4-right). For every position boundary, a 20% energy window was set automatically.

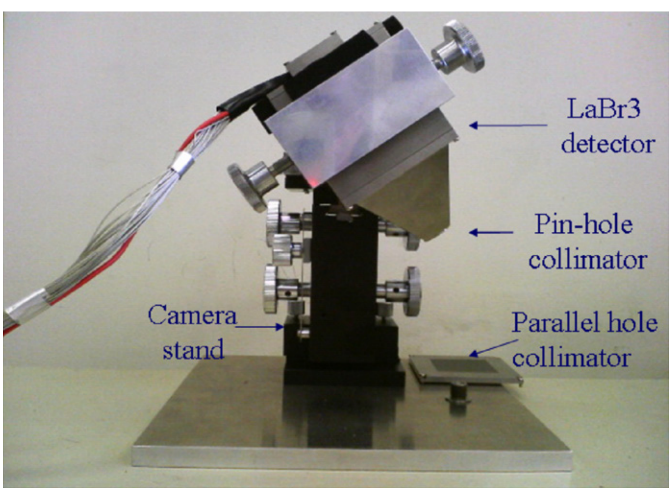

Fig. 5. Photograph of LaBr3(Ce) gamma camera system with pinhole collimator.

Fig. 5 shows a photograph of the $LaBr_3$(Ce) gamma camera system with a pinhole collimator. The detector part is encased in a 5 mm tungsten-based alloy (heavy metal) shield, and a pinhole collimator was mounted in front of the detector surface. The pinhole collimator was made of a tungsten-based alloy (heavy metal) whose diameter was 0.5 mm and positioned 50 mm from the detector surface. The collimator was replaceable, and a parallel hole collimator could also be attached. The detector part was suspended by a camera stand that could move in the *X*, *Y*, and *Z* directions and can also be rotated. The size of the gamma camera system is approximately $20\,\text{cm} \times 20\,\text{cm} \times 20\,\text{cm}$ and weight is approximately 5 kg.

2.2. Performance measurements

(1) Energy resolution
The energy spectra were measured without a collimator by irradiating the detector surface uniformly with Co-57 (122 keV) and Am-241 (60 keV) gamma photons. The energy spectrum was measured for the entire FOV without energy correction. Energy signal (summed signals for all PSPMT anodes) was fed to an NIM-based amplifier and a multi-channel analyzer (MCA). Energy resolution was calculated using the Gaussian fit for the energy distribution.

(2) Intrinsic spatial resolution
The intrinsic spatial resolution was measured using a 2 mm thick tungsten slit phantom with 1 mm slits positioned on the detector (Fig. 6(A)). The distance between the neighboring slits was 4 mm. Gamma photons from Co-57 (122 keV) or Am-241 (60 keV) point source located approximately 20 cm from the detector surface were employed, and images were taken in the high spatial resolution accumulation mode. Profiles of the line source image were set to evaluate the spatial resolution. Corrected intrinsic spatial resolution for the slit width (R_{corr}) was performed using the following equation [4,15,16]:

$$R_{corr} = (R_m^2 \text{-} W_s^2)^{1/2}$$

where R_m is the measured intrinsic spatial resolution, and W_s is the slit width of the mask (1 mm)
The intrinsic spatial resolution was also evaluated using a 2 mm thick bar pattern phantom that has four sectors of slits whose slit widths were 1.2, 1.0, 0.8, and 0.6 mm (Fig. 6(B)). The center to center spacing of these slits was twice the slit width. Gamma photons from Co-57 (122 keV) or Am-241

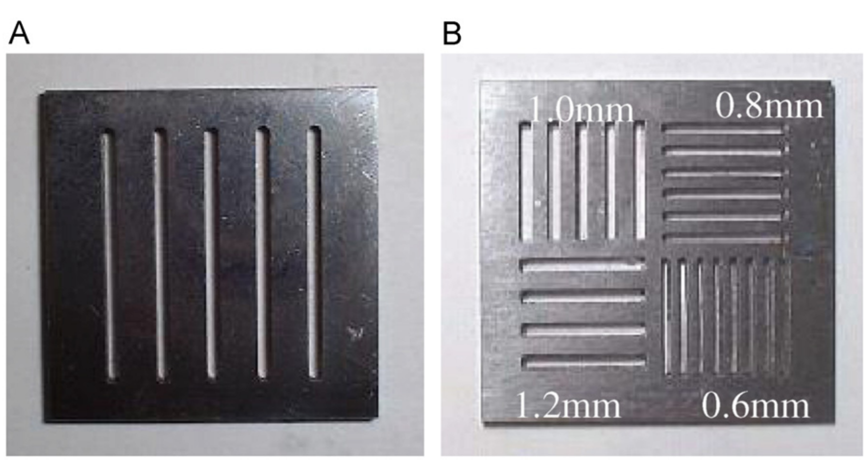

Fig. 6. Photographs of slit phantom (A) and bar pattern phantom (B).

(60 keV) point sources located approximately 20 cm from the detector surface were employed. Images were taken in the accumulation mode.

(3) Sensitivity
Sensitivity with pinhole collimator was evaluated for gamma photons from Co-57 (122 keV) as a function of the distance from the collimator surface. A point source of radioactivity approximately 1.85 MBq (50 μCi) and size less than 1 mm was positioned in front of the pinhole collimator and the count rate was measured by changing the distance between collimator surface and the point source in 5 mm step from 0 to 30 mm.

(4) Image quality
The image quality in the corrected mode was measured using several phantoms. Because the purpose of this work is to demonstrate the developed gamma camera can really work for many types of subjects, most of the image quality evaluation was performed visually. The image of a spatial linearity phantom was measured using a 2 mm thick tungsten plate with 1 mm square slits arranged in the phantom (Fig. 7(A)). The spatial resolution for the corrected mode was measured using the same bar pattern phantom shown in Fig. 6(B). The flood image was taken to verify the image

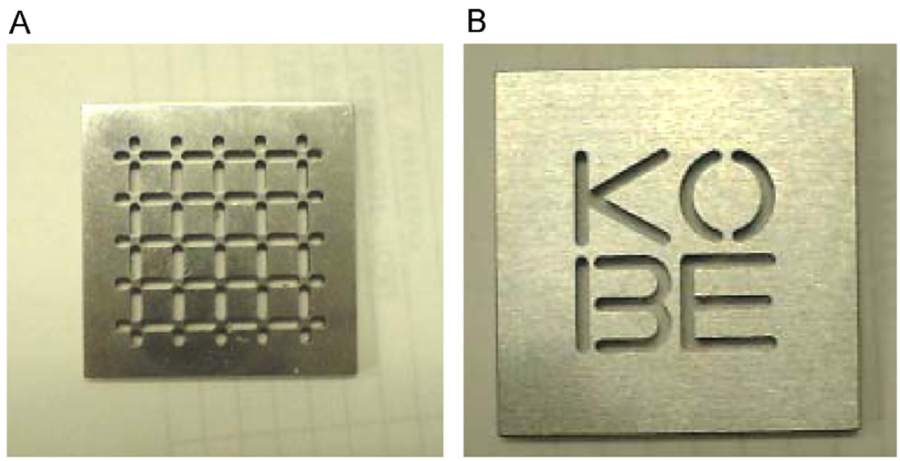

Fig. 7. Photographs of spatial linearity phantom (A) and "KOBE" phantom (B).

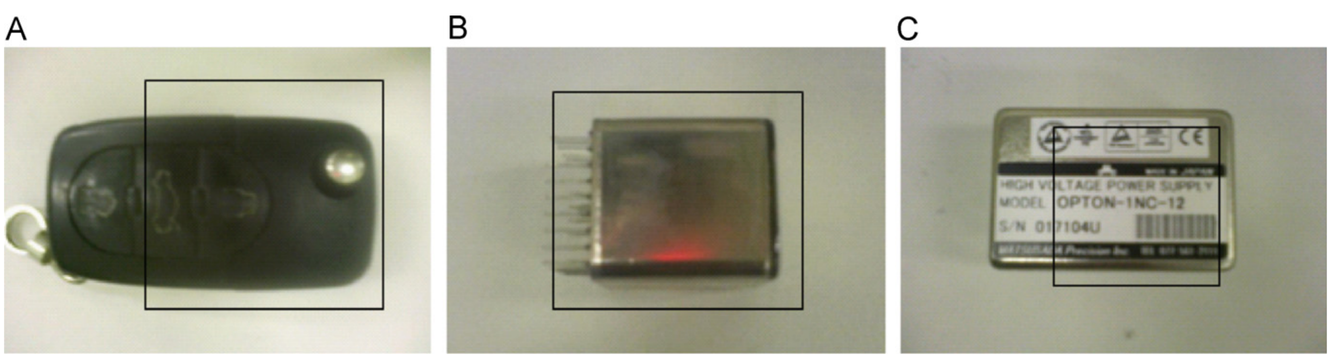

Fig. 8. Photographs of objects for transmission imaging: electrical car key (A), 1 in. metal PSPMT (B), and small high voltage supply (C). Squares in the figures are imaged portions of objects.

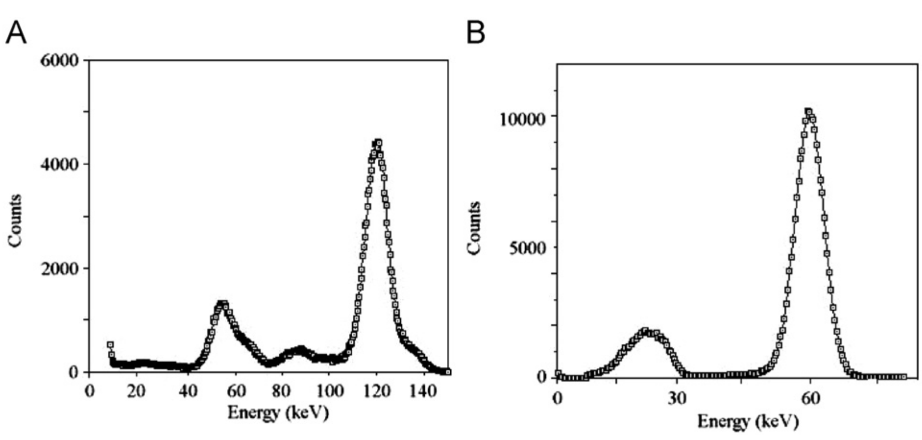

Fig. 9. Energy spectra of $LaBr_3$(Ce) gamma camera for Co-57 gamma photons (122 keV) (A) and Am-241 gamma photons (60 keV) (B).

uniformity without a mask on the detector surface. Image uniformity was also visually evaluated. The overall image quality was visually evaluated using the "KOBE" tungsten mask with slits of characters that were 1 mm wide (Fig. 7(B)). The distance between the separated parts in "*O*" and "*B*" is less than 0.5 mm. For all measurements, gamma photons from Co-57 (122 keV) point sources positioned approximately 20 cm from the detector surface were employed.

(5) Transmission images
To demonstrate the high resolution image of the detector, the transmission images of electrical components were measured. Three types of objects positioned on the detector without collimator and gamma photons from Co-57 (122 keV) point sources were irradiated approximately 8 cm from the detector surface. The radioactivity of the Co-57 was approximately 1.85 MBq (50 μCi). The acquisition time was 10 min for each image. The photographs of the objects are shown in Fig. 8: an electrical car key (AUDI A6), an one-inch metal position sensitive PMT (Hamamatsu H9500), and a small high voltage supply (Matsusada, OPTON-INC-12)

(6) Emission images of phantom and rat
The emission image of a phantom was measured using a "hot phantom" with six sectors of holes of 1.25, 1.5, 1.75, 2.0, 2.25, and 2.5 mm. The center to center distances between holes were twice of the diameters of the holes. The Tc-99 m solution whose radioactivity was approximately 370 kBq (100 μCi) was contained in the phantom and imaged by the detector with a pinhole collimator. The distance between the phantom and the collimator surface was approximately 20 mm.
To demonstrate the high resolution capability of the $LaBr_3$(Ce) gamma camera, an emission image of a rat chest was measured. Approximately 20 MBq (0.54 mCi) of Tc-99 m hydroxymethylene diphosphonate (HMDP) was intravenously administered to a normal male Wistar rat from the tail vein under anesthesia. The study was performed under the guidelines of the Laboratory Investigation Committee of the Osaka University Graduate School of Medicine. The rat was imaged by the detector with a pinhole collimator. The distance between the rat to the collimator surface was approximately 20 mm. The acquisition time was 420 min.

2.3. Long term stability

Long term stability is important for this type of scitillator with hygroscopic character. Approximately two years after the fabrication of the detector, a flood image was measured using the 122 keV gamma photons from Co-57, uniformly irradiated from approximately 10 cm above the detector and compared with that measured approximately two months after fabrication.

3. Results

(1) Energy resolution
Fig. 9 shows the energy spectra of the $LaBr_3$(Ce) gamma camera for Co-57 (122-keV) and Am-241 (60 keV) gamma photons. The energy resolution was 8.9% FWHM for Co-57 and 13.4% FWHM for Am-241.

(2) Intrinsic spatial resolution
Fig. 10 (A) and (B) shows slit images obtained by the developed gamma camera without a collimator using Co-57 and Am-241, respectively. The profiles for these images are shown in Figs. 10(C) and (D). The spatial resolution for the

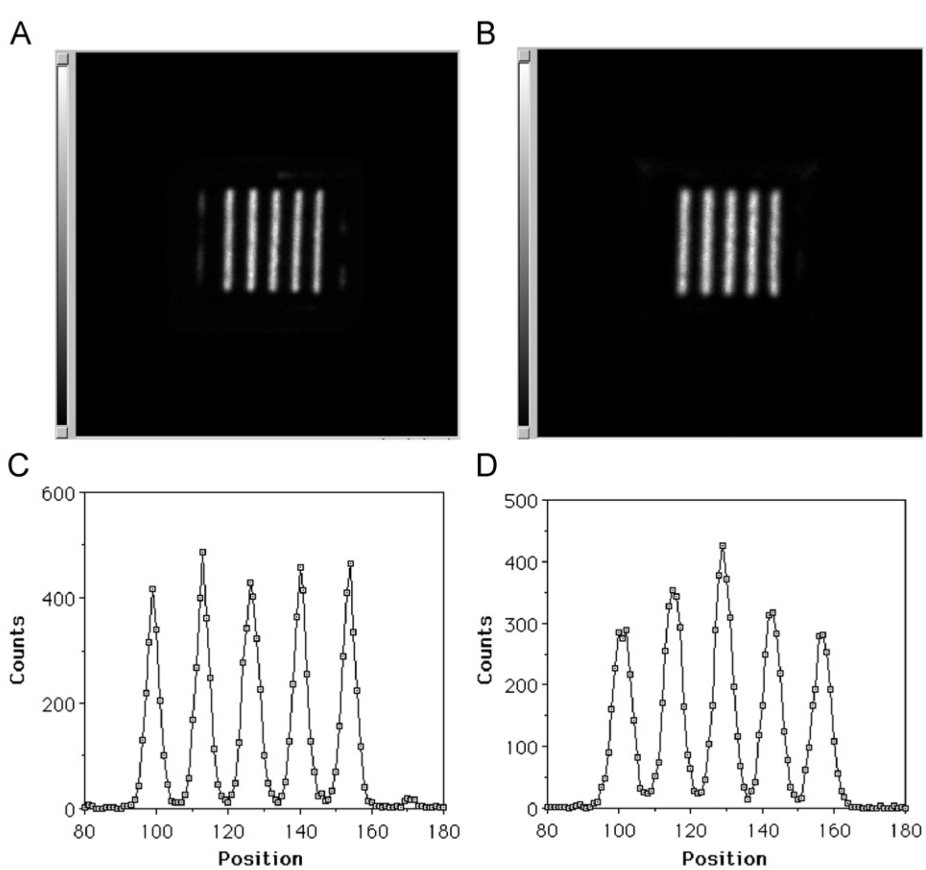

Fig. 10. Image of slit phantom for Co-57 gamma photons (122 keV) (A), Am-241 gamma photons (60 keV) (B), profile of image for Co-57 (C), and that for Am-241 (D).

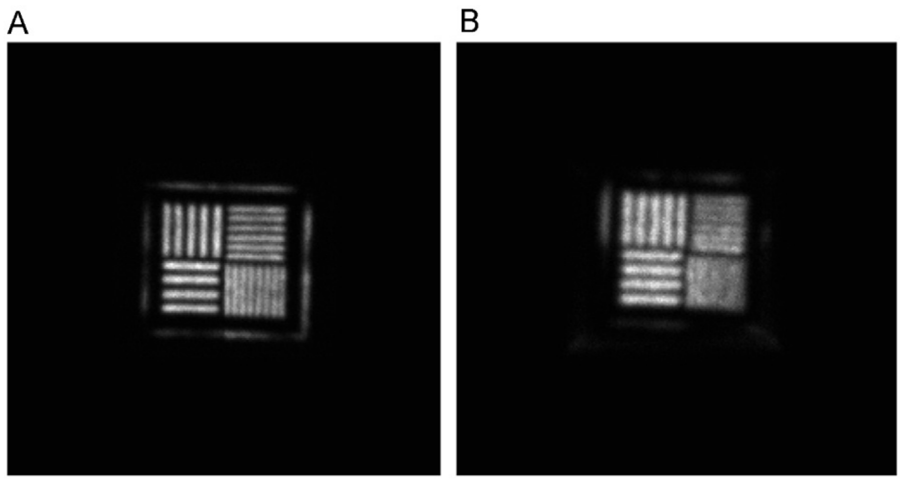

Fig. 11. Images bar pattern phantom for Co-57 (A) and for Am-241(B).

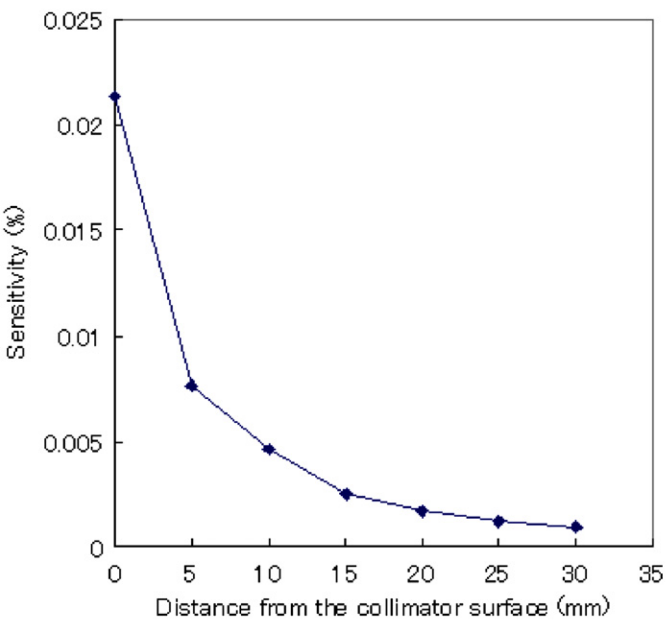

Fig. 12. Sensitivity as a function of distance from the collimator surface.

Co-57 gamma photons was 0.75 mm FWHM, and that for Am-241 was 1.4 mm FWHM after the correction of the physical slit width (1 mm).

The images of bar pattern phantom for Co-57 and for Am-241 are shown in Figs. 11(A) and (B), respectively. In the image of Co-57, the smallest bars (0.6 mm) were clearly resolved. For the image of Am-241, the 0.8 mm bars were almost resolved.

(3) Sensitivity

Sensitivity as a function of distance from the collimator surface is shown in Fig. 12. Sensitivity was 0.0047% at 10 mm and 0.0017% at 20mm from the collimator surface.

(4) Image quality

An image of the spatial linearity phantom is shown in Fig. 13(A). The image shows good linearity because the linearity error was within one pixel of the image (1 mm). The image of the bar pattern phantom in the corrected mode is shown in Fig. 13(B). The spatial resolution was degraded compared to the accumulation mode due to the large pixel size. In the corrected mode, 0.6–0.8 mm slits were resolved.

The flood image, which is shown in Fig. 13(C), shows good uniformity and has no observable systematic non-uniformity. The image of the "KOBE" phantom is shown in Fig. 13(D). The characters as well as the separated parts of "*O*" and "*B*" are clearly observed.

(5) Transmission images

The transmission images of an electrical car key, 1 in. metal PSPMT, and small high voltage supply are shown in Fig. 14(A), (B) and (C), respectively. Here the inside structures of the metals and electrical parts are observed.

(6) Emission images of a phantom and a rat

Fig. 15(A) shows the image of the hot spot phantom. All the spots in the central part are clearly resolved. Fig. 15(B) shows the image the chest part of rat to which Tc-99 m HMDP was administered. The bone structure of the chest is clearly observed in the image.

3.1. *Long term stability*

Flood images of Co-57 measured at approximately two month (A) and two years (B) after the fabrication are shown in Fig. 16. The flood image showed significant distortion due to the change in $LaBr_3$(Ce) of its hygroscopic characteristic. Almost half area of the FOV produced no signal (black part of the image).

4. Discussion

We developed a high spatial resolution gamma camera using $LaBr_3$(Ce) combined with PSPMT. The thickness of the $LaBr_3$(Ce) scintillator used for the detector was 2 mm, not thick enough to absorb most of the Tc-99 m gamma photons; approximately 40% of the gamma photons are absorbed [7]. Although increasing scintillator thickness increases the detection efficiency of the gamma camera, it also decreases the intrinsic spatial resolution of the detector because the light spread of the detector increases [5]. Consequently, some compromise must be made between the detection efficiency of the scintillator and the intrinsic spatial resolution. This compromise can be seen in the commercial gamma camera; a thicker scintillator with a high detection efficiency gamma camera has lower intrinsic spatial resolution [17].

In the gamma camera, a light guide is sometimes used between the scintillator and PMT or PSPMT to reduce the

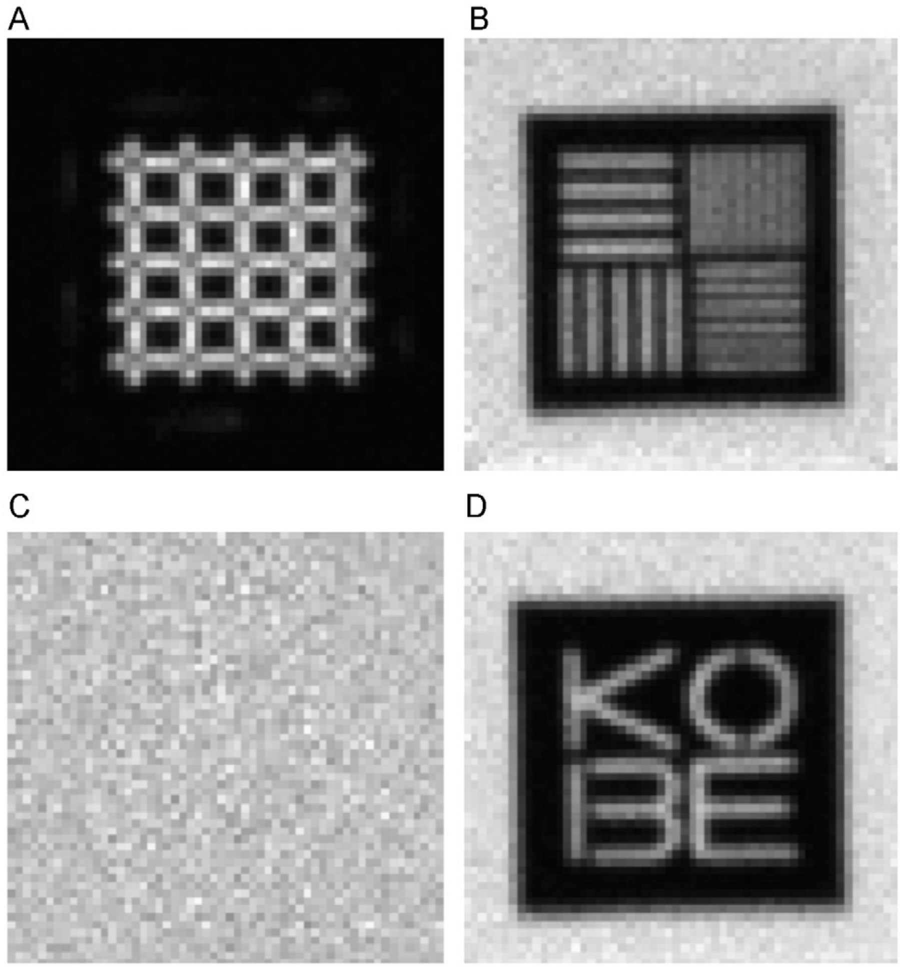

Fig. 13. Images of spatial linearity phantom (A), bar pattern phantom (B), flood image (C), and "KOBE" phantom (D).

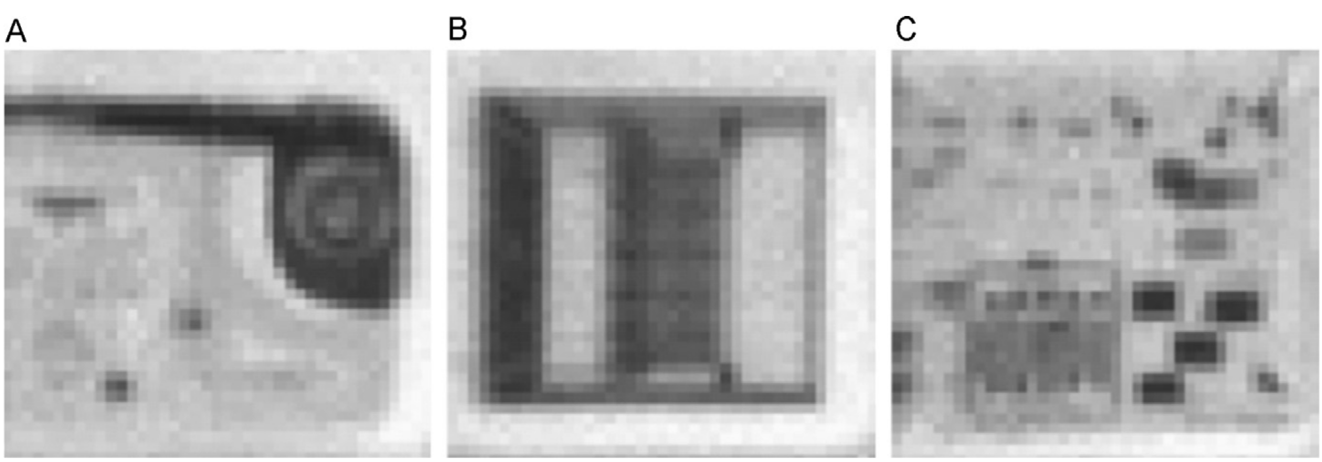

Fig. 14. Transmission images of electrical car key (A), 1 in. metal position sensitive PMT (B), and high voltage supply (C).

non-uniformity and the spatial distortion of the image. In the developed detector, no light guide was employed. However, no serious non-uniformity or distortion was observed even in the accumulation mode image (Fig. 4 middle). One reason is that the glass envelope of the PSPMT (3 mm thick) acted as a light guide to distribute the scintillation photons among the PSPMT anodes. Another reason is that the size of the PSPMT anode was relatively small (6 mm $\times$ 6 mm) compared to the thickness of the scintillator (2 mm) plus the glass of the PSPMT (3 mm).

The energy resolution of our camera system is better than other scintillation cameras using an NaI(Tl) scintillator and a PSPMT. The energy resolution was 14% FWHM for the NaI(Tl) based gamma camera used PSPMT without fiber plate for Co-57 (122 keV) gamma photons [5], so the energy resolution of

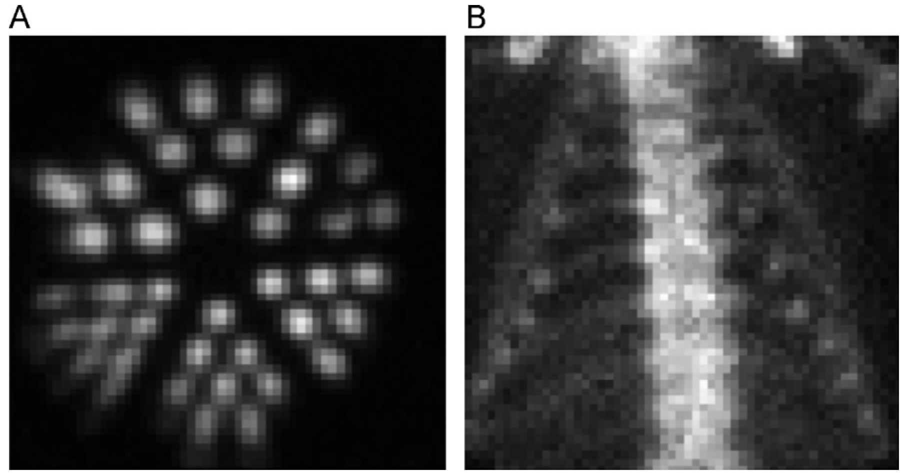

Fig. 15. Images: hot spot phantom (A) and bone image of rat (B).

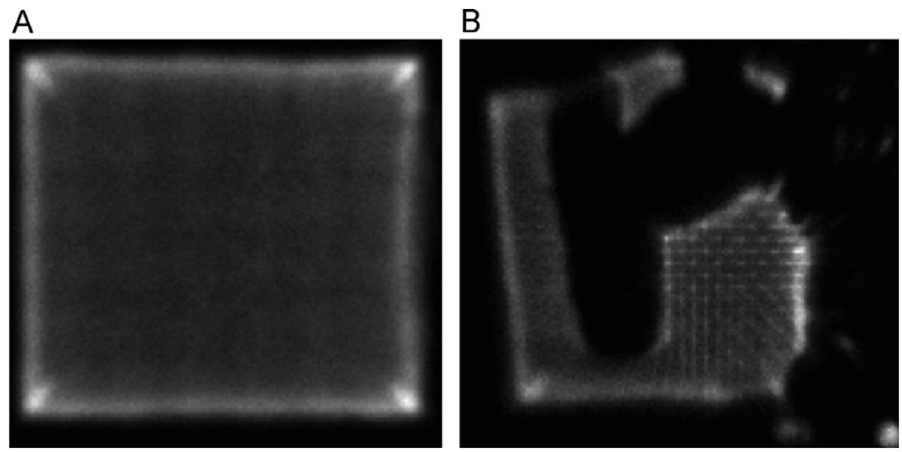

Fig. 16. Flood image of the detector of approximately 2 month (A) and two years after fabrication.

developed $LaBr_3$(Ce) gamma camera is approximately 36% better than that of the NaI(Tl) based gamma camera. The energy spectrum presented in Fig.9 was the total energy without energy correction and the energy resolution was 8.9% FWHM. With energy correction, energy resolution will be better because the presented energy resolution is degraded by the energy peak variation of the position of the detector, although the gain variations of the PSPMT anodes are to be of almost equal level.

In our developed gamma camera system, the intrinsic spatial resolution with the corrected mode is determined by the size of the pixels. The image matrix size of the corrected mode is limited to a maximum of 64×64 by the hardware of the data acquisition system used for the camera. If the size of the pixel could be smaller by increasing the matrix size, the intrinsic spatial resolution would be equal to the accumulation mode.

The biggest problem of the developed gamma camera is the long term stability. Two years after fabrication of the detector by the manufacture, more than half area of the FOV produced no signals. However, degradation of the detector seems to be started long before this time. All data except long term stability were measured within two months after fabrication of the detector. It is thought that the degradation of the detector started after this time and gradually worsens. The reason of the degradation is the strong hygroscopic characteristic of $LaBr_3$(Ce). The direct coupling of the $LaBr_3$(Ce) to the FP-PMT and relatively high humidity of the country (Japan) may be the additional reasons of this relatively early degradation of the detector.

5. Conclusion

We conclude that the developed high spatial resolution $LaBr_3$(Ce) gamma camera is promising for small animal imaging using a low energy single photon emitting radionuclide if the hygroscopic problem of the $LaBr_3$(Ce) will be solved.

Acknowledgement

This research was partially supported the National Institute of Biomedical Innovation.

References

[1] D.A. Weber, M. Ivanovic, J. Nucl. Cardiol. 6 (1999) 332.
[2] F.J. Beekman, F. von der Have, Eur. J. Nucl. Med. Mol. Imaging 34 (2007) 151.
[3] T. Aoi, T. Zeniya, H. Watabe, H.M. Deloar, T. Matsuda, H. Iida, Ann. Nucl. Med. 20 (2006) 245.
[4] G. F. Knoll, Radiation Detection and Measurement, 2nd edition (1989).
[5] S. Yamamoto., IEEE Trans. Nucl. Sci. NS-53 (1) (2006) 49.
[6] E. van Loef, P. Dorenbos, C.W.E. van Eijk, Appl. Phys. Lett. 79 (10) (2001) 1573.
[7] Saint-Gobain, BrilLanCe 380 data sheet.
[8] K. Kuhn, S. Suirti, J.S. Karp, et al., IEEE Trans. Nucl. Sci. NS-53 (3) (2006) 1090.
[9] R. Pani, R. Pellegrinia, M.N. Cintia, P. Bennatia, M. Bettia, V. Casalia, et al., Nucl. Instr. and Meth. Phys. Res. Sec. A 569 (2006) 296.
[10] R. Pani, R. Pellegrinia, M. Bettia, G. De Vincentisa, M.N. Cintia, et al., Nucl. Instr. Meth. Phys. Res. Sec. A 571 (2007) 475.
[11] H. Kudo, K. Hattori, C. Iida, S. Iwaki, S. Kabuki, S. Kurosawa, T. Nagayoshi, et al., Development of a gamma camera based on an 8×8 of $LaBr_3$(Ce)

scintillator pixels coupled to a 64 channel multi-anode PMT., Nuclear Science Symposium Conference Records, 2007.
[12] A. Abe, N. Takahashi, J. Lee, T. Oka, K. Shizukuishi, T. Kikuchi, T. Inoue, M. Jimbo, H. Ryuo, C. Bicke, Eur. J. Nucl. Med. Mol. Imaging 30 (6) (2003) 805.
[13] H. Kim, L.R. Furenlid, M.J. Crawford, D.W. Wilson, H.B. Barber, T.E. Peterson, et al., Med. Phys. 33 (2) (2006) 465.
[14] S. Yamamoto, K. Matsumoto, M. Senda., Phys. Med. Biol. 51 (2006) 457.
[15] C.S. Levin, E.J. Hoffman, M.P. Tomai, L.R. MacDonald., IEEE Trans. Nucl. Sci. NS-44 (4) (1997) 1513.
[16] J.E. Lees, D. Bassford, G.W.D. Fraser, M. Monk, R.J.Ott EarlyI. Moody, E. Blackshaw, A.C. Perkins, IEEE Trans. Nucl. Sci. NS-53 (1) (2006)9.
[17] T. Inoue, N. Oriuchi, K. Koyama, A. Ichikawa, K. Tomiyoshi, N. Sato, et al., Ann. Nucl. Med. 15 (2001) 141.